

**GT2011-4\* , \$+**

## **SEPARATION CONTROL USING PLASMA ACTUATORS: STEADY FLOW IN LOW PRESSURE TURBINES**

**Debashish Burman**  
University of Minnesota  
Minneapolis, MN, USA

**Terrence W. Simon**  
University of Minnesota  
Minneapolis, MN, USA

**Uwe Kortshagen**  
University of Minnesota  
Minneapolis, MN, USA

**Douglas Ernie**  
University of Minnesota  
Minneapolis, MN, USA

### **ABSTRACT**

A Dielectric Barrier Discharge plasma actuator is operated in flow over the suction surface of a Pack-B Low Pressure Turbine (LPT) airfoil at a Reynolds number of 50,000 (based on exit velocity and suction surface length) and inlet free-stream turbulence intensity of 2.5%. Measurements of total pressure using a glass total-pressure tube are taken. Corrections for streamline displacement due to shear and wall effects are made, and comparisons with previous hot-wire measurements are used to validate data. Measurements from previous work have shown that separation control is possible without stream-wise momentum addition, by adding disturbances that cause transition in the separated shear layer. The present results are from measurements taken using a glass dielectric, with a conventional two-electrode geometry, and a new three-electrode geometry. The region of high momentum flow produced due to the presence of the actuator is found to be above the shear layer, and not at the wall. The near-suction-surface total pressure field in the trailing part of the airfoil passage and its wall-normal gradient are used to demonstrate effective prevention of flow separation using the plasma actuator.

### **INTRODUCTION**

The low pressure turbine (LPT) section of a gas turbine comprises the last few stages of turbomachinery for work extraction from the flow before it is passed through a nozzle (aircraft engine) or released to the atmosphere (stationary power generator). In a modern aircraft engine, the low pressure turbine is typically constrained to operate at low rotational speed, equal to that of the intake fan. In operation, a low pressure turbine

experiences low chord-based Reynolds numbers, typically in the range of  $0.5$  to  $5 \times 10^5$  [Howell 2000]. In this Reynolds number range, an unsteady, transitional boundary layer may be found over a major part of the airfoil suction surface, and flow separation is likely. The drop in lift and increase in losses accompanying separation causes a large drop in efficiency.

The LPT accounts for 20-30% of the engine weight [Hodson and Howell, 2005]. An effort to reduce weight and cost for each component drives a reduction in blade count per stage, leading to higher blade loading and increased likelihood of separation. Design is strongly driven toward peak performance under sea-level take-off conditions. At cruise conditions at higher altitudes, the decrease in flow Reynolds number causes a component efficiency drop of 2-7%, with the lower figure representative of commercial aircraft engines, and the higher figure representative of smaller engines at higher altitudes [Hultgren and Ashpis, 2003]. The overall specific fuel consumption of the engine is a strong function of LPT performance. A 1% increase in LPT polytropic efficiency results in a 0.5-1% drop in fuel consumption [Wisler, 1998]. A 1% reduction in jet fuel consumption is estimated to be worth \$1.25M per day [Seifert et al., 2002].

Large portions of the suction surface boundary layer of a low pressure turbine stage are laminar or transitional. Transition to turbulence may occur before or after separation, depending on the airfoil geometry, flow Reynolds number and free-stream turbulence level. Transition to turbulence in separated shear layers can lead to partial or complete re-attachment.

Turbulence levels in low pressure turbines range from 2 to 10% [Simon and Kaszeta, 2001]. When the free-stream turbulence levels are high (greater than about 1% [Morkovin, 1984; Suder et al., 1988]), the natural instability modes and initial stages of boundary layer growth are bypassed, with direct excitation of turbulent spots. This is the so-called “bypass transition” mode which is relevant to low pressure turbine flows. Volino [2002] observed turbulence spectra from measurements taken in a low pressure turbine suction surface boundary layer at a high free-stream turbulence level (9%), where bypass transition is the relevant mode. A broad-band nature was evident, as opposed to non-bypass cases at low FSTI, which showed distinct peaks at frequencies associated with shear-layer instability.

Separation control strategies in LPTs can be passive or active. Passive control devices, such as dimples [Bearman and Harvey, 1993] and fixed turbulators [Lin et al., 1994], have been a traditional approach to re-energizing the flow by triggering transition and inducing re-attachment, but create parasitic drag at take-off and high Reynolds number conditions [Volino, 2003], when they are not required. Active control devices can be employed only when needed.

Plasma actuators and vortex generating jets (VGJs) are prominent subjects of recent research in active flow control. Active control mechanisms may lend themselves to separation control by one of two modes: a) adding near-wall momentum and stabilizing the flow as it encounters the adverse pressure gradient, thereby delaying or preventing separation, or b) inducing the laminar boundary layer or separated shear layer to undergo transition to turbulence by introducing disturbances that lead to rapid growth of ambient disturbances.

Pulsed control is frequently attempted. Depending on the nature of the dominant mode of transition, specific frequencies or broad-band excitation may be effective. It is difficult to find consensus about the most effective frequency (or bands of frequencies), in either case. One study [Mayle, 1998] concluded that the most effective forcing frequency in the free-stream for bypass transition is  $1.3U/(2\pi\eta)$ , where  $U$  is the free-stream velocity, and  $\eta$  is the Kolmogorov length scale. Others [e.g., Bons, 2002] find that a broad range of low frequencies is capable of forcing effective flow control. [Halfon et al., 2004] experimentally studied leading edge separation of a flat plate, and found that higher free-stream turbulence levels and introduction of two-dimensional periodic excitations led to thinner, shorter separation bubbles. Excitation waves comparable to length of the original bubble were less effective than waves that were shorter (by about a factor of three). An increase in FSTI produced a decrease in the net effectiveness of the periodic excitation.

The application of Dielectric Barrier Discharge (DBD) plasma flow control was demonstrated by Roth et al. [1998],

and has been developed over the last decade via computational, experimental, and theoretical research approaches spanning from fundamental studies of the discharge to a wide range of applications [e.g., Hultgren and Ashpis, 2003; Enloe et al., 2004; Opaitis et al., 2005; Corke et al., 2007].

A DBD actuator comprises an arrangement of two electrodes separated by a dielectric (insulator) that encapsulates one of them, with the other electrode exposed to the surrounding air. When a large, high frequency ( $\sim$ kV,  $\sim$ kHz) time-varying voltage is applied between the electrodes, the surrounding fluid is weakly ionized, producing a plasma. The discharge produces a faint bluish-purple emission, which is visible in a dark room or in long-exposure photographs.

Although this plasma appears to be a uniform and diffuse glow, it has considerable temporal and spatial structure. The plasma is stable at normal atmospheric conditions and has a self-limiting nature, i.e. it quenches itself at any constant applied voltage and requires a time-varying voltage to sustain a discharge. The effect of the plasma on a surrounding fluid is a result of collisional momentum transfer from ions and electrons to the neutral fluid molecules, and is not a thermal effect for typical kHz-range AC, DBD discharges [Orlov, 2006].

Careful control of the actuator geometry and driving voltage characteristics leads to an active flow controller. It draws relatively little power and does not suffer the usual drawbacks of added weight, mechanical vibration, complexity, poor dynamic response of other active control devices or the parasitic drag loss associated with passive control solutions.

Previous work by the authors [Burman et al., 2010] has shown that stream-wise momentum addition is not required for separation control, i.e., adding only disturbances to the shear layer may suffice. This was done by orienting the actuator so that momentum was imparted to the flow opposite to the stream-wise direction and comparing the results to a case with momentum imparted to the flow in the streamwise direction. For effective scaling of plasma actuators for separation control to real engine flows, it is important that the energy for delaying or preventing separation, or inducing early re-attachment come from the flow itself, with the actuator providing only the disturbance that triggers transition in the shear layer. If momentum addition near the wall were to be the primary mode of separation control, the velocity produced by the actuator must scale up from laboratory flows to the engine in proportion to the free-stream. Such high velocities from plasma actuators have not been demonstrated.

Burman et al. [2010] also found that enhanced separation control was associated with span-wise edge effects of actuators. In agreement with [Volino 2002] and consistent with characteristics of bypass transition, no specific pulsing frequencies of interest were found.

## NOMENCLATURE

$d$	=	dia. of total pressure tube
$\delta_w$	=	wall displacement correction
$FSTI$	=	free-stream turbulence intensity
$L_{ss}$	=	total suction surface length
$LPT$	=	low pressure turbine
$\nu$	=	coefficient of kinematic viscosity
$pp$	=	peak-to-peak amplitude
$\rho$	=	fluid density
$rms$	=	root mean square
$Re_{L_{ss}}$	=	$(L_{ss} \cdot U_{exit}) / \nu$ , Reynolds number
$s$	=	stream-wise extent along suction surface
$T_u, TI$	=	$u'_{rms} / U_{inlet}$ , inlet free-stream turbulence intensity
$\tau_w$	=	wall shear stress
$U$	=	free-stream velocity
$u$	=	local stream-wise velocity
$u_\tau$	=	skin-friction velocity = $\sqrt{\tau_w / \rho}$
$v$	=	local wall-normal velocity
$w$	=	local span-wise velocity
$x$	=	axial distance from blade leading edge
$y$	=	wall-normal dimension
$'$	=	fluctuating component

## EXPERIMENTAL SETUP, INSTRUMENTATION AND UNCERTAINTY

Separation control is studied using a Pratt & Whitney Pack-B (sometimes spelled in the literature as Pak-B) low pressure turbine airfoil passage. Figure 1 shows a schematic of the wind tunnel and the airfoil passage.

A low-speed, open-return wind tunnel is used. The facility is equipped with filters for preventing damage to thermal sensors, a honeycomb flow straightener section for swirl removal, a heat exchanger section for fine spatial and temporal control of flow temperature, a screen-pack and settling chamber, a 10.7:1 contraction nozzle, and a jet-grid turbulence generator for control of inlet flow turbulence intensity. In various configurations, this facility can produce between 0.5% and 20% inlet free-stream turbulence intensity.

One suction surface and one pressure surface form the single passage test section used for this study. Adjustable bleed slots are located in the passage approach duct. Tufts are used for confirming stagnation on the leading edge of the blade. Static pressure measurements from taps located on the suction surface are used to confirm agreement with the high Reynolds number Pack-B pressure profile. Tailboards were originally attached to the section, but were later found unnecessary and removed. Further details on the test section may be found in Simon et al., [2000].

The Reynolds number  $Re_{L_{ss}}$  for this study is 50,000. In this study, the grid generator is used in passive mode, i.e., not blown, to produce an inlet free-stream turbulence intensity of

2.5%. These conditions may be considered to be representative of flight at cruising altitudes, especially in smaller engines.

The suction surface of the airfoil is machined to permit a 1.3 mm thick glass dielectric to be flush-mounted on the suction-surface. A mandrel machined to the shape of the suction surface is used to slump a glass plate in an oven to conform to this airfoil shape. Figure 2 and Table 2 summarize the dimensions of the airfoil.

The plasma actuator is constructed by attaching electrodes to both sides of the glass dielectric. A schematic is shown in Fig. 3. The single electrode on the non-flow side of the dielectric is encapsulated with insulating film, so that no plasma discharge is formed on that side. In our case, this electrode is the grounded electrode, and is also referred to as the second electrode. The powered electrode on the flow side of the dielectric immediately upstream of the grounded electrode is referred to as the first electrode. In this study, a third electrode is also present. It is on the flow side of the dielectric, and downstream of both the first and second electrodes. The third electrode is connected to the first electrode through a diode.

Each electrode is a strip of copper tape that is 0.08 mm thick (wall-normal direction) and 6.4 mm wide (stream-wise direction). The trailing edge of the first electrode is aligned with the leading edge of the second electrode, and is 10 mm upstream of the leading edge of the third electrode.

When only the first and second electrodes are activated, it is referred to as a two-electrode configuration, which is the standard configuration for most plasma actuator flow controllers. When all three electrodes are active, it is a three-electrode configuration.

A glass tube with an outer diameter of 1.25 mm is used as a total pressure tube. All total pressure measurements are relative to the passage exit static pressure, which is open to atmospheric pressure. A picture of one such tube is shown in Fig. 4. While metal tubes with smaller diameters are readily available, arcing has been observed in the vicinity of the discharge and the charged dielectric. An arc-like discharge can affect the local velocity field, thus affecting the measured total pressure. We mention in passing that strong electric fields in the vicinity of the discharge can also affect seeding particles associated with Laser-Doppler Velocimetry (LDV) and Particle-Image Velocimetry (PIV), as well as smoke particles in flow visualizations. Informal testing with a hot-wire anemometer shows that the anemometer signal can be contaminated by the high-carrier signal frequency of the actuator, which is picked up by the probe acting as an antenna. Further processing and/or filtering of hot-wire is then required.

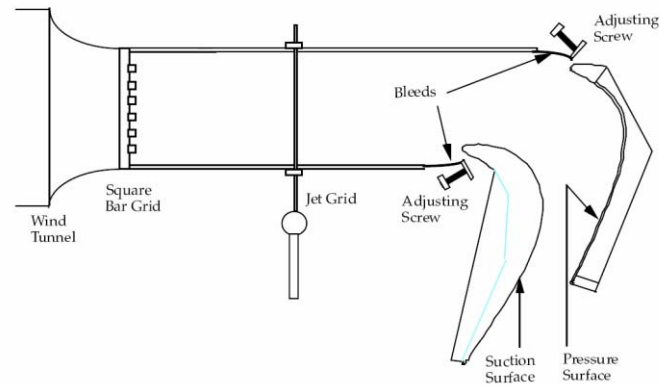
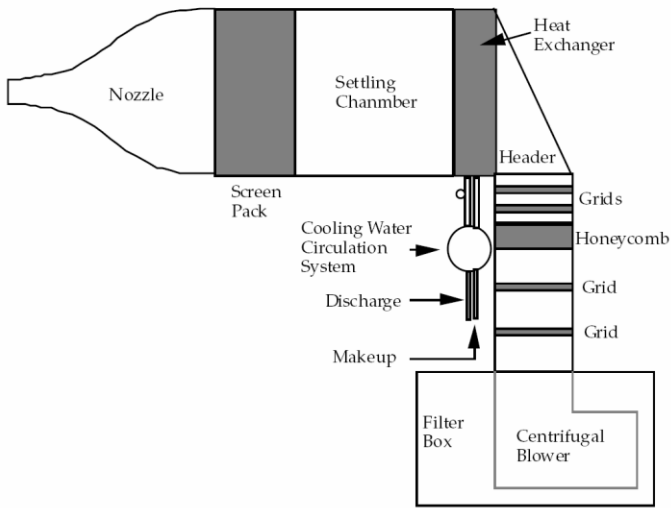


**Figure 1. Schematic showing the low-speed wind tunnel (top), and the development section and Pack-B passage, as attached to the end of the nozzle (bottom) [Simon et al., 2000].**

A Dwyer 1430 Microtector<sup>®</sup> micromanometer is used for measurement of pressure from the total pressure tube. It is specified to be precise to  $12.8 \times 10^{-3}$  mm (0.00050 inch) of water column pressure, and has a 0 to 50.8 mm (0 to 2 inches) of water column pressure range. A computer-controlled National Aperture Micromini<sup>®</sup> traverse is used to translate the tube normal to the wall.

The waveform produced for this study is a 9 kHz, 14.7 kV<sub>pp</sub> sine wave, which is pulsed at 80 Hz with a 0.6 duty cycle. A Tektronix AFG 3022B arbitrary function generator produces the continuous or intermittent waveform of interest, which is amplified by a Trek PD05034 high voltage amplifier. A Tektronix P6015A high-voltage probe is used to measure the actuator voltage.

With 95% confidence, the uncertainty in measurements from the total pressure tube is less than 5%.

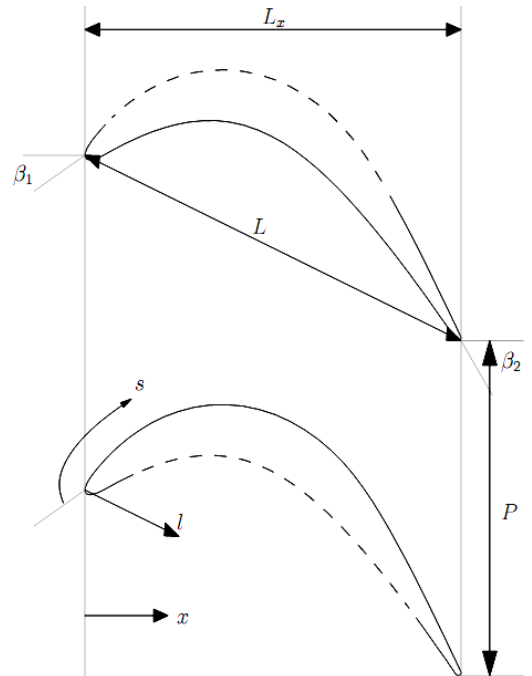


**Figure 2. Schematic showing Pack-B turbine passage dimensions [Kaszeta et al., 2003].**

Chord length, $L$	114.3 mm
Axial chord length, $L_x$	103.57 mm
Suction surface length, $L_{ss}$	152.76 mm
Axial chord to chord ratio, $L_x/L$	0.906
Pitch to chord ratio, $P/L$	0.8
Aspect ratio (span/chord), $L/L$	6.0
Blade inlet angle, $\beta_1$	35°
Blade outlet angle, $\beta_2$	-60°

**Table 1. Dimensions of the Pack-B turbine passage [Kaszeta et al., 2003].**

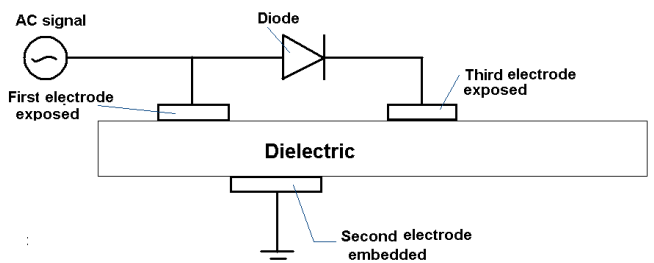


**Figure 3. Schematic showing the actuator arrangement for the three-electrode geometry. Flow is from left to right.**

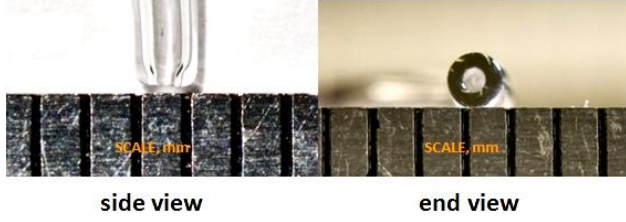


**Figure 4. Glass total pressure tube used for total pressure measurements. The relevant scale is adjacent to each view of the tube, in millimeters.**

### CORRECTIONS FOR PRESSURE MEASUREMENTS

Near the wall, the blockage effect of a pressure tube causes streamline displacement, which produces a lower velocity measurement than is accurate. Additionally, when a pressure tube is placed in a shear flow with a positive velocity gradient, as in a boundary layer, the tube registers a higher velocity than is accurate. Figure 5 shows a schematic of these effects. Well-known corrections exist for these effects, which oppose each other in a typical attached wall-bounded flow.

A simple and popular formulation is due to [MacMillan, 1954]. In a shear flow, the correction applied to the wall-normal distance  $y$  of the probe is constant, given by

$$\frac{\Delta y}{d} = 0.15 \quad (1)$$

Near the wall, for  $y/d < 2$ , the correction is applied to velocity instead of wall-normal distance, given by

$$\frac{\Delta u}{u} = 0.015 \exp \left[ -3.5 \left( \frac{y}{d} - 0.5 \right) \right] \quad (2)$$

Equations 1 and 2 are meant to be applied near the wall additively.

McKeon et al. [2003] also suggest a formulation for pitot tube displacement and wall correction, which was also evaluated for the present study. Their displacement correction for shear is given by

$$\frac{\Delta y}{d} = 0.15 \tanh(4\sqrt{a}) \quad (3)$$

where

$$a = \frac{d}{2u_{truecenterline}} \frac{du}{dy} \Big|_{centerline} \quad (4)$$

is a measure of the local velocity gradient.

Their proposed wall correction is based on a correction to  $y$ , rather than to  $u$ , unlike the MacMillan wall correction. If the correct pressure is read at

$$y = 0.5d \left( 1 + \frac{\delta_w}{d} \right), \quad (5)$$

$\delta_w$  being the wall displacement correction, then  $\delta_w/d$  equals 0.15 for  $d^+ < 8$ , 0.12 for  $8 < d^+ < 110$ , and 0.085 for  $110 < d^+ < 1600$ , with  $d^+ = du_\tau/\nu$ , and  $u_\tau = \sqrt{\tau_w/\rho}$ .

Viscous corrections (due to low probe-diameter Reynolds number) were evaluated but not applied, since the correction was found to be negligible relative to the uncertainty in measurement.

Shear-stress visualizations and hot-wire data from previous studies [Simon et al., 2000] show that when the pressure tube resides within the separation bubble in a zone of possible reversed flow, the velocities are low enough ( $\approx 0$ ) for the effect of this back flow to be negligible. Unsteadiness levels are high relative to the local velocity within the separation bubble, but the absolute velocities have been measured to be near zero and, thus, the velocity fluctuations are also small in an absolute sense. As expected, unsteadiness corrections were found to be negligible in this case.

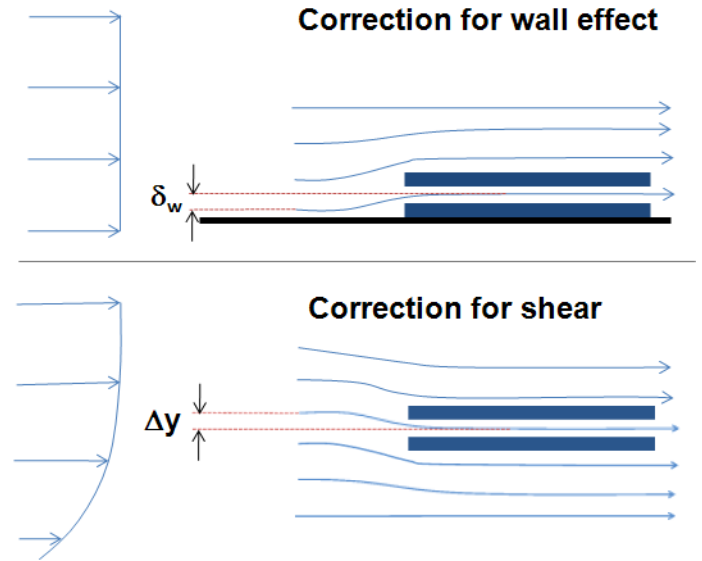


**Figure 5. Schematic showing streamline displacement due to the presence of the wall, and due to shear.**

## RESULTS AND DISCUSSION

Hot-wire velocity data from [Simon et al., 2000] that were taken under identical conditions, but without the actuator present, were used for comparison and validation of the total pressure measurements from the present study.

Figure 6 shows the comparison of these hot-wire data with total pressure measurements from the present study converted to velocity, both taken at stream-wise location  $s/L_{ss} = 0.55$ , which is in the vicinity of incipient separation. The hot-wire profile shown in the figure indicates that the flow is still attached. The wall static pressure used for computing the velocity was found by extrapolating the total pressure profile to the wall. There is significant stream-line curvature due to the airfoil passage geometry, causing the static pressure to increase away from the wall. The wall-normal gradient of static pressure was found from the free-stream wall-normal velocity gradient of the hot-wire data.

The displacement and wall corrections [McKeon et al., 2003] were applied to the data shown in Fig. 6. Evaluating the corresponding corrections [MacMillan, 1954] produced results that are very similar to those seen in Fig. 6. In both cases, good agreement is seen.

Stream-wise locations downstream of separation have wall-normal gradients of static pressure that vary according to the radius of the local streamline curvature. In particular, after the separated shear layer has undergone transition to turbulence and re-attachment is imminent, the static pressure in the shear layer increases toward the wall, which is opposite to the sense of the static pressure gradient farther upstream. Figure 7 shows a sketch of this phenomenon.

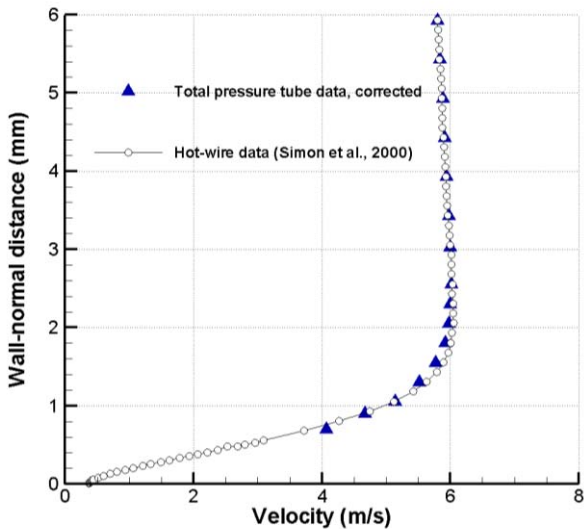


**Figure 6. Comparison of the corrected total pressure tube measurements with hot-wire data [Simon et al., 2000]. This stream-wise location of  $s/L_{ss} = 0.55$  corresponds to incipient separation.**

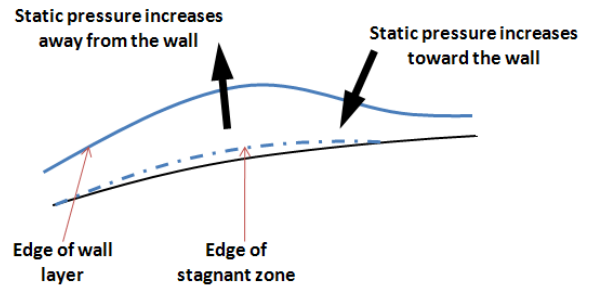


**Figure 7. Schematic showing the change in sense of the static pressure gradient when the flow begins to turn toward the wall before re-attachment.**

For illustration, a typical total pressure profile taken in separated flow ( $s/L_{ss} = 0.76$ , well downstream of separation) and converted to velocity is shown in Fig. 8. The maximum velocity from the corresponding hot-wire measurement of [Simon et al., 2000] was compared to the constant total pressure in the free-stream from the present study to compute the static pressure at the interface of the shear layer and free-stream. In this case, this corresponds to a wall-normal distance  $y \approx 5.3$  mm. The static pressure increases for  $y > 5.3$  mm due to stream-line curvature in the free-stream, which is found from the slope of the hot-wire velocity profile in that zone and applied to the velocities calculated from total pressure, as shown in the plot. The static pressure also increases for  $y < 5.3$  mm, because the flow begins to turn toward the wall before re-attaching farther downstream. This situation corresponds to the downstream arrow of Fig. 7. For Fig. 8, the velocities calculated from total pressure for  $y < 5.3$  mm used the constant static pressure at  $y \approx 5.3$  mm, producing the disparity shown. Calculation using an estimated radius of curvature for the re-attaching streamline indicates that the magnitude of the disparity at the wall seen in Fig. 8 is reasonable. It is simple to evaluate this static pressure gradient if the hot-wire data are used in conjunction with the total pressure measurements.

While all total pressure measurements from the present study could be converted to velocity with the use of the hot-wire data of Simon et al. [2000] to compute static pressure gradients, the above was primarily an exercise in validation of the present measurements. Total pressure, itself, is a reasonable parameter for evaluating separation control. For this study, the total pressure measurements are therefore not converted to velocity, but presented after correction for displacement due to shear and wall effects, as applicable. A wall-normal gradient of the total pressure is also computed, and is found to be a useful quantity for visualizing the zones of viscous losses in the flow (i.e. shear and boundary layers).

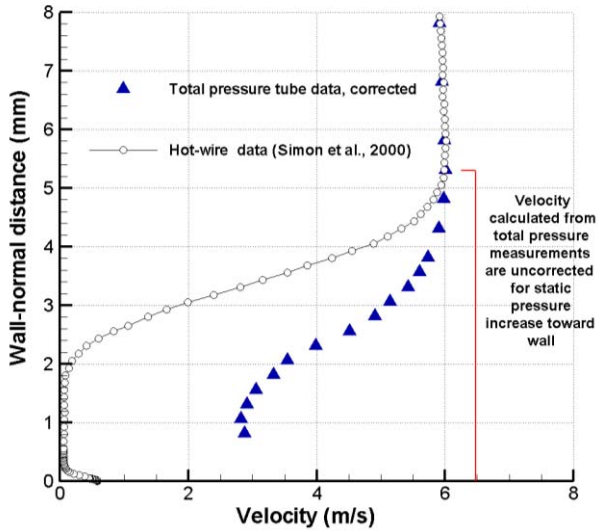


**Figure 8. Comparison of the corrected total pressure tube measurements with hot-wire data [Simon et al., 2000]. The flow is separated at this  $s/L_{ss} = 0.76$  station, and static pressure increases toward the wall from the edge of the shear layer near the free-stream (not corrected for)**

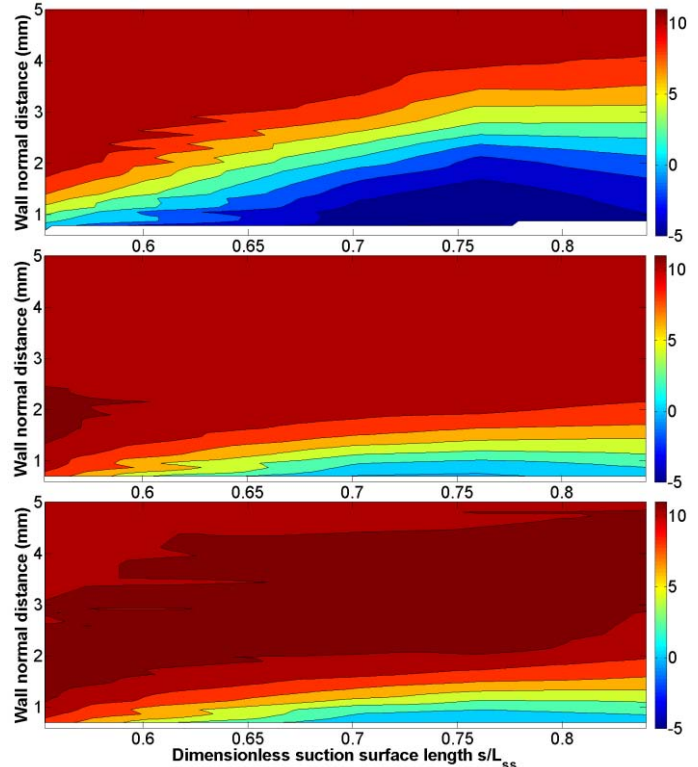
In all cases, the downstream edge of the first electrode is at a non-dimensional stream-wise distance  $s/L_{ss} = 0.49$ . Measurement of total pressure profiles are made at five stream-wise stations, having  $s/L_{ss} = 0.55, 0.61, 0.70, 0.76,$  and  $0.84$ .

Figure 9 shows the plot of total pressure in the trailing part of the suction surface of the Pack-B airfoil. The top figure shows the field with the actuator off, i.e., it is the base case for the chosen Reynolds number and inlet turbulence intensity. The separation of the laminar wall layer is seen at the extreme left of the plot. The separated layer continues to leave the wall until transition to turbulence occurs, after which the enhanced transport of momentum produces growth of the separated shear layer and shrinking of the separation zone. Re-attachment occurs farther downstream than the right edge of the plot, very near the trailing edge of the airfoil.

The middle plot of Fig. 9 shows the total pressure field when the two-electrode geometry actuator is activated. The third electrode is present in this case, but not electrically connected. The boundary layer continues to thicken, but separation is not evident in the figure. It is possible that a small separation bubble exists below the field of measurement. The high total pressure zone, seen near the left edge of the middle plot in dark red 2 mm away from the wall, is a region of accelerated flow produced when the actuator's zone of influence is encountered by the free-stream as a "virtual bump". Note that this high momentum region is not actually at the wall and is in fact above the shear layer, i.e., it is not directly increasing the wall shear stress by adding momentum to the near-wall flow to delay separation. It is expected that early

transition due to the pulsed disturbance added to the shear layer by the actuator is primarily responsible for the absence of separation (or the very thin separation zone).

The three-electrode geometry produces a stronger zone of high momentum than the two-electrode case, with peak velocities higher than those of the free-stream, as shown in the bottom plot of Fig. 9. It produces a thinner attached boundary layer over the suction surface than that for the two-electrode configuration (or a very thin separation zone).



**Figure 9. Total pressure (Pa) in the trailing part of the low pressure turbine passage, with the actuator off (top), on in the two-electrode configuration (middle), and on in the three-electrode configuration (bottom).**

The mechanism for the greater thrust due to an active third electrode may be explained as follows. The potential due to the third electrode helps to re-distribute the surface charge (that accumulates on the dielectric) toward the downstream direction. The modified electric field lines lead to increased acceleration of charged particles in the stream-wise direction, which transfer this additional momentum to the neutral air molecules by collisions [Guo, 2010].

Based upon an understanding of the first electrode inducing flow along the stream-wise direction, it may appear that the discharge due to the third electrode must induce flow in the direction opposite to the free-stream flow, at least partially counteracting the effects of the first discharge. In practice,

visual observation indicates that if any discharge at the third electrode exists, it is extremely weak, and we expect that any effect on the flow due to the third electrode's discharge is also very weak. The major effect of the third electrode is the redistribution of surface charge that accumulates on the dielectric, rather than a direct effect on the flow due to an additional discharge.

For this study, we expect little or no discharge activity at the third electrode, for two reasons:

a) Distance: the electrode configuration used for this study features a grounded electrode that is not directly beneath the third electrode, but about 3 mm upstream of it. For 3 kV/mm breakdown voltage in air, it would take about 9 kV of voltage difference between the third electrode and the charged dielectric to produce a discharge.

b) Available voltage: the occurrence of  $\Delta V \approx 9$  kV would be a much more infrequent event for the third electrode compared to the first electrode, since the applied signal as seen by the third electrode is the rectified positive half of the applied AC sinusoidal signal. For the required voltage difference to be available between the third electrode and the dielectric, we would need to operate at signal amplitudes greater than 18 kV<sub>pp</sub>, which is higher than what has been used for this study.

As mentioned previously, we have connected actuators in both forward and reversed configurations without a diode in the circuit in the past, which allows both configurations to have nominally identical discharges. Our observation was that the reversed case (with the flow induced upstream, against the flow) was also effective in separation control, although somewhat less so than the case with the stream-wise oriented induced flow. We concluded from this experiment that stream-wise momentum addition is not a requirement for flow control, and control authority is attainable using disturbance-based control.

While the third electrode is seen to be the more effective of the two geometries, it can limit the performance of the two-electrode geometry in its present configuration. This is because the signal amplitude that can be used with the third electrode present is limited by initiation of arcing between the two exposed electrodes. A purely two-electrode configuration would have no such limitation. An optimally located third electrode would increase the stream-wise momentum coupled by the discharge into the flow, but would be far enough from the first electrode to prevent arcing.

The wall-normal gradient of the total pressure is plotted in Fig. 10. Zones of high shear are visible as areas of high positive total-pressure gradient, indicated in red. Separation of the shear layer can be seen in the case with the actuator off (top), while it appears to remain attached in the two- and three-electrode cases (middle and bottom). As mentioned before, it is possible that a thin separation bubble exists very near the wall. Additionally, the high momentum region formed due to the presence of the

actuator is visible as a dark blue streak in the two cases with the actuator activated.

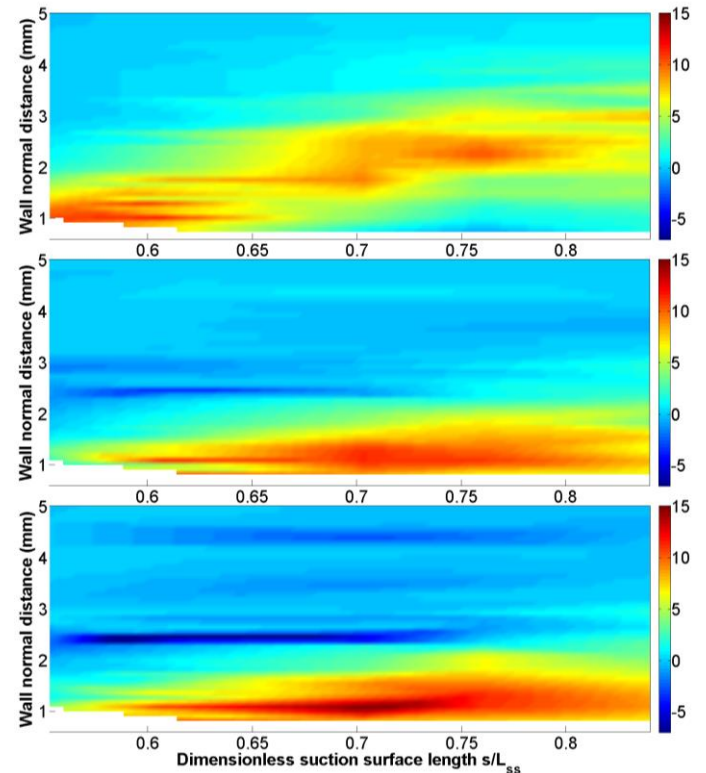


**Figure 10. Wall-normal gradient of total pressure (Pa/mm) in the trailing part of the low pressure turbine passage, with the actuator off (top), on in the two-electrode configuration (middle), and on in the three-electrode configuration (bottom).**

## CONCLUSIONS

The efficiency of the low pressure turbine strongly affects the overall engine efficiency, with suction surface separation being the primary contributor toward losses in the LPT. Incremental improvements have major implications, most directly for engine fuel consumption, weight and cost.

The present work demonstrates effective control of separation in a Pack-B low pressure turbine geometry using a plasma actuator in two different configurations. The first configuration uses a buried grounded electrode located downstream of an exposed energized electrode. The other configuration adds a third electrode downstream of the first two electrodes. This third electrode is connected to the first exposed electrode when the latter is at a higher potential than the former, via a diode. The inlet flow conditions, with Reynolds number  $Re_{L_{ss}}$  of 50,000 and inlet free-stream turbulence intensity of 2.5%, may be considered to be representative conditions for a small engine at cruise conditions.

Total pressure measurements were taken with a glass total pressure tube, corrected for streamline displacement due to wall and shear effects, and validated using previous hot-wire data. Results are plotted as fields of total pressure (Pa) and wall-normal gradient of total pressure (Pa/mm) in the near-suction-surface trailing part of the passage.

Both configurations show fully attached flow (or very thin separation zones) when the actuator is activated. The three-electrode configuration is somewhat more effective than the two-electrode configuration. The presence of the third electrode can limit performance by direct arcing, depending upon the applied signal and the distance between the exposed electrodes. Both configurations produce zones of high momentum flow directed away from the wall, formed when the free-stream encounters and is diverted by the presence of the “bump” formed by the actuator.

The greater effectiveness of the three-electrode configuration is attributed to surface charge re-distribution due to the third electrode, leading to increased stream-wise acceleration of the charged particles in the plasma, which is imparted to the neutral fluid by collisions.

## ACKNOWLEDGMENTS

This work is funded by NASA Glenn Research Center, under NASA Cooperative Agreement NNX07AB94A. We thank Philip Poinsette and David Ashpis, both of NASA, for their support.

## REFERENCES

Bearman, P. W., and Harvey, J. K., “Control of circular cylinder flow by the use of dimples,” *AIAA Journal*, October 1993

Bons, J. P., Sondergaard, R., and Rivir, R. B., “The Fluid Dynamics of LPT Blade Separation Control Using Pulsed Jets,” *ASME J. Turbomachinery*, 124, 2002

Burman, D., Simon, T. W., Kortshagen, U., and Ernie, D., “Separation control using plasma actuators: 2-D and edge effects in steady flow in low pressure turbines,” *AIAA 2010-1220*, 2010

Corke, T. C., Post, M. L., and Orlov, D. M., “SDBD Plasma Enhanced Aerodynamics: Concepts, Optimization and Applications,” *Prog. Aero. Sciences*, Vol. 43, 2007

Enloe, L., McLaughlin, T., VanDyken, R., Kachner, K., Jumper, E., and Corke, T., “Mechanisms and Response of a Single Dielectric Barrier Plasma Actuator: Plasma Morphology,” *AIAA J.*, Vol. 42, 2004

Guo, S., private communication, 2010

Halfon, E., Nishri, B., Seifert, A., and Wygnanski, I., “Effects of elevated free-stream turbulence on actively controlled separation bubble,” *Journal of fluids engineering*, 2004

Hodson, H. P., “Aspects of Unsteady Blade-Surface Boundary Layers and Transition in Axial Turbomachines,” *Boundary Layers in Turbomachines*, VKI Lecture Series 1991–2006, 1991

Hodson, H. P., and Howell, R. J., “Blade row interactions, transition, and high-lift airfoils in low-pressure turbines,” *Ann. Rev. of Fluid Mech.*, 37, 2005

Hultgren, L. S. and Ashpis, D. E., “Demonstration of Separation Delay with Glow-Discharge Plasma Actuators,” *AIAA Paper 2003-1025*, 2003

Kaszeta, R. W., Simon, T. W., Ottaviani, F., and Jiang, N., “The Influence of Wake Passing Frequency and Elevated Free Stream Turbulence Intensity on Transition in Low-pressure Turbines,” *AIAA Paper 2003-3633*, 2003

Lin, J. C., Robinson, S. K., McGhee, R. J., and Valarezo, W. O., “Separation control on high-lift airfoils via micro-vortex generators,” *Journal of Aircraft*, 31, 1994

MacMillan, F. A., “Viscous effects on Pitot tubes at low speeds,” *J. R. Aero. Soc.*, 58, 1954

MacMillan, F. A., “Experiments on Pitot tubes in shear flow,” *Ministry of Supply, Aero. Res. Council R & M 3028*, 1956

Mayle, R. E., Dullenkopf, K., and Schulz, A., “The Turbulence That Matters,” *ASME J. Turbomachinery*, 120, 1998

McKeon, B. J., Li, J., Jiang, W., Morrison, J. F., and Smits, A. J., “Pitot probe corrections in fully developed turbulent pipe flow,” *Meas. Sci. Technology*, 14, 2003

Morkovin, M., “Bypass Transition to Turbulence and Research Desiderata,” *Transition in Turbines*, NASA Conf. Publ. 2386, 1984

Opaits, D., Roupasov, D., Starikovskaia, S., Starikovskii, A., Zavalov, I. and Saddoughi, S., “Plasma Control of Boundary Layer using Low-Temperature Non-Equilibrium Plasma of Gas Discharge,” *AIAA Paper 2005-1180*, 2005

Orlov, D. M., “Modelling and simulation of single dielectric barrier discharge plasma actuators,” *Dissertation*, University of Notre Dame, 2006

Roth, J. R., Sherman, D. and Wilkinson, S., "Boundary Layer Flow Control with One Atmosphere Uniform Glow Discharge Surface Plasma," 36th Aerospace Sciences Meeting and Exhibit, Reno, NV, AIAA-98-0328, 1998

Seifert, A., Theofilis, V., and Joslin, R. D., "Issues in Active Flow Control: Theory, Simulation and Experiment," AIAA Paper 2002-3277, June 2002

Simon, T. W., and Kaszeta, R. W., "Transition to turbulence under low-pressure turbine conditions," Annals of the New York Academy of Sciences, 934, 2001

Simon, T. W., Qiu, S., and Yuan, K., "Measurements in a transitional boundary layer under low-pressure turbine airfoil conditions," NASA/CR-2000-209957

Suder, K. S., O'Brien, J. E., and Reshotko, E., "Experimental Study of Bypass Transition in a Boundary Layer," NASA Tech. Memorandum 100913, 1988

Volino, R. J., "Separated Flow Transition Under Simulated Low-Pressure Turbine Airfoil Conditions: Part 1—Mean Flow and Turbulence Statistics," ASME J. Turbomachinery, 124, 2002

Volino, R. J., "Separated Flow Transition Under Simulated Low-Pressure Turbine Airfoil Conditions: Part 2—Turbulence Spectra," ASME J. Turbomachinery, 124, 2002

Volino, R. J., "Separation Control on Low-Pressure Turbine Airfoils Using Synthetic Vortex Generator Jets," ASME Paper 2003-GT-38729, 2003

Yajnik, K. S., and Gupta, R. P., "A new probe for measurement of velocity and flow direction in separated flows," J. Phys. E: Sci. Instrum., 6, 1973

Wisler, D. C., "The technical and economic relevance of understanding Blade Row interactions effects in turbomachinery," von Karman Institute for Fluid Dynamics Lecture series 1998-02, February 9-12, 1998